Validation of Clyde River SuperDARN radar velocity measurements with the RISR-C incoherent scatter radar

Alexander Koustov[1], Robert Gillies[2] and Peter Bankole[1]

[1]University of Saskatchewan, Saskatoon, Saskatchewan, Canada

5   [2]University of Calgary, Calgary, Alberta, Canada

Correspondence to: A.V. Koustov (sasha.koustov@usask.ca)

Abstract

The study considers simultaneous plasma velocity measurements in the eastward direction carried
10   out by the Clyde River SuperDARN HF radar and Resolute Bay incoherent scatter radar RISR-C.
The HF velocities are found to be in reasonable agreement with RISR velocities up to magnitudes
of 700-800 m/s while for faster flows, the HF velocity magnitudes are noticeably smaller. The
plasma flows eastward component inferred from SuperDARN convection maps (constructed for
the area of joint measurements) shows the effect of smaller HF velocities even at smaller velocities.
15   We show that the differences between the instruments can be significant and prolonged for
observations of strongly-sheared plasma flows.

1 Introduction

20   The Super Dual Auroral Radar Network (SuperDARN) HF radars have been installed to
continuously monitor the $\mathbf{E} \times \mathbf{B}$ plasma drift in the Earth's ionosphere (Greenwald et al., 1995).
To achieve this goal, the radars measure Doppler velocity of ionospheric echoes coming from the
F region. The return signal, in this case, is coherent backscatter from decameter irregularities that
move with the velocity close to the plasma $\mathbf{E} \times \mathbf{B}$ drift. A number of comparisons of SuperDARN
25   velocity measurements with concurrently operating incoherent scatter radars (ISR) that measure
the plasma $\mathbf{E} \times \mathbf{B}$ drift has been performed in the past (Ruohoniemi et al., 1987; Davis et al., 1999;
Milan et al., 1999; Xu et al., 2001; Gillies et al., 2009; Gillies et al., 2010; Bahcivan et al., 2013;
Koustov et al., 2016; Gillies et al., 2018). These observations, overall, supported the above major

assumption of the SuperDARN principle in plasma flow measurements. However, occasional

30   significant differences between HF radar line-of-sight (LOS) velocity and $\mathbf{E}\times\mathbf{B}$ drift component along the beam have been noticed. Initially, these were thought to originate from differences in the echo collecting areas (Davies et al., 1999) but the body of the data, published so far, questions this notion. It is accepted now that the HF velocities are generally smaller (Gillies et al., 2018). One identified effect leading to this result is the fact the SuperDARN measurements are done under an

35   assumption that the medium has the index of refraction of unity. However, this explanation cannot account for large differences of more than 20-30%. Koustov et al. (2016) stressed the original finding by Xu et al. (2001) that the HF velocity magnitudes substantially smaller (up to a factor of 2) than the $\mathbf{E}\times\mathbf{B}$ drift component for high-speed flows of >1000 m/s. Furthermore, often the HF velocity magnitudes are above the $\mathbf{E}\times\mathbf{B}$ component (e.g. Ruohoniemi et al., 1987; Koustov et al.,

40   2016; Gillies et al., 2018). Such observations have been interpreted in terms of lateral deviation of HF radar beams (Koustov et al., 2016; Gillies et al., 2018). Some SuperDARN-ISR velocity inconsistencies have been associated with the occurrence of E region echoes at traditionally expected F region ranges for SuperDARN (Bahcivan et al., 2013; Gillies et al., 2018).

Despite an obvious progress, HF-based $\mathbf{E}\times\mathbf{B}$ measurements require further investigation

45   if one wants to further improve the quality of the convection mapping with HF radars. In addition, although all SuperDARN radars work on the same principle and often even have identical hardware, validation work for every unit is highly desirable to be confident in reliability and consistency of measurements across the network.

In this study, we undertake a validation work for the Clyde River (CLY) SuperDARN

50   radar. In a broader context, this effort is a complementary one to the previous validation work for the Rankin Inlet (RKN) and Inuvik (INV) SuperDARN radars by Koustov et al. (2009), Mori et al. (2012), Bahcivan et al. (2013), Koustov et al. (2016) and Gillies et al. (2018). Since currently the CLY radar contributes significantly to the global-scale convection mapping with SuperDARN such work is of particular importance. We take here an advantage of the availability of the $\mathbf{E}\times\mathbf{B}$

55   drift measurements with recently installed incoherent scatter radar RISR-C (Canada) at Resolute Bay (RB), e.g. Gillies et al. (2016). An important aspect of the present work is that we compare CLY and ISR-based velocities in a different way as compared to the previous studies.

Traditionally, gate-by-gate comparison of data from two radar systems making measurements in roughly the same directions is performed, e.g. Gillies et al. (2018). Such an

60   approach cannot be implemented for the CLY/RISR-C geometry because none of these radars'
beams are close enough (see map on Fig. 1 in Gillies et al. (2018)). For this reason, we consider
RISR-C two-dimensional vectors in a certain area (which are inferred by merging data from
multiple individual beams using the approach by Heinselman and Nicolls (2008)) and compare
them with highly-averaged CLY data (over 3 beams and 4 gates). Thus, we assess the data in a

65   statistical sense, in terms of the average (median) velocities over a large space domain.

To further substantiate our reasoning, we remind the reader that SuperDARN global-scale
maps of plasma flow obtained with the Potential Fit technique (Ruohoniemi and Baker, 1998;
Shepherd and Ruohoniemi, 2000) are built using median-filtered LOS velocities, the so-called
gridded velocities. These are inferred from up to 27 raw velocity LOS values (if available) in

70   certain beam/gate and in ± one range gate for ± one radar beam and for ± one radar scan. This
implies that what eventually goes into the Potential Fit procedure is a highly smoothed HF velocity
covering 3-6 min of raw data and a significant space domain. In this view, there is a sense in
considering 2-D RISR-C data and compare them with HF velocity medians, or vectors from the
convection maps, over large spatial areas of overlap.

75   Although our aim is to validate the CLY velocity measurements, there is additional value
for the CLY-RISR comparison. The RISR method of velocity vectors estimations has some
limitations as well (Heinselman and Nicolls, 2008) and the technique employed needs testing by
itself. A couple of the limitations are a lack of velocity measurements along magnetic field lines
and the expectation of spatially quasi-uniformity of flows, which is not always satisfied. Thus, our

80   work can be considered as a mutual validation of both radar system performance. Compatibility
of the vector estimates by RISR and SuperDARN is highly expected, but to what degree has not
been reported so far.

2 Geometry of RISR-C and Clyde River radar observations

85

Figure 1 shows the fields of view (FOV) of the CLY and RKN SuperDARN radars starting from
range gate 5 and the location of the RB incoherent scatter radar RISR-C, which we will simply
refer to as the RISR radar starting from here. This radar makes measurements in multiple beams;
it uses 11 beams in the so-called "world-day" mode and 51 beams in the so-called "imaging" mode.

90   Measured line-of-sight velocities in all the beams and at all ranges are used to infer 2-D vectors of

the **E×B** flow according to the procedure outlined by Heinselman and Nicolls (2008). The resultant vectors are reported with $0.25°$ step of magnetic/geographic latitude. The points where the measurements are assigned are roughly shown in Fig. 1 (for the height of 300 km). The actual center line for the points of data merging depends on data availability in specific beams (Gillies et al., 2018).

95
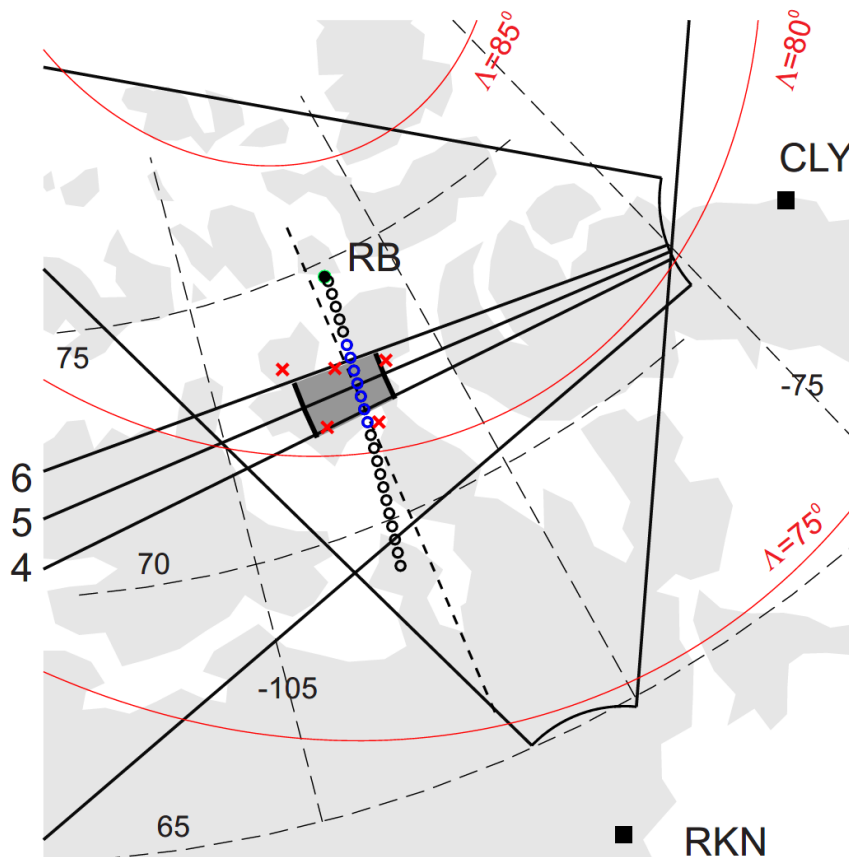
Figure 1: Field of view of the SuperDARN radar at RKN and CLY. The black straight lines are the orientation of specific beams (4-6 for CLY) whose data were investigated. Shaded areas represent areas of HF radar data averaging. RB is the location of the RISR-C incoherent scatter radar. The radar reports **E×B** vector with a step of $0.25°$ of geographic latitude for points shown as black circles stretching roughly along the magnetic meridian crossing the RB zenith. The blue-colored circles are those locations whose data were used for comparison with the CLY measurements. The solid red lines are the magnetic latitudes of $75°, 80°$ and $85°$.

105   Figure 1 also shows the orientation of the CLY beams 4, 5, 6 (their centers) and the area where data were considered, the shaded rectangle outlined by beams 4 and 6 between range gates

18-22. The monitored ionospheric region is centered at geographic latitude of $\sim 72.5°$. An important feature of this area is that here the CLY beams 4-6 are almost parallel to the lines of equal geographic latitude at the chosen radar range gates, as seen in Fig. 1. This means that one

110   can directly compare CLY LOS velocity and the Eastward component (in geographic coordinates, as given by RISR) of a RISR $\mathbf{E} \times \mathbf{B}$ velocity vector. We note that the area of CLY observations was also covered by measurements from the RKN and INV radars so that SuperDARN convection maps were usually well constrained.

115   **3 Methodology of the LOS velocity comparison**

We consider here an extensive data set comprising of RISR observations over the entire year 2016. Overall, about 1,000 hours of RISR measurements were available. The radar typically worked for 24 hours switching, once-in-a-while, its mode of operation, except the world-day mode which

120   usually covered an entire day. The range resolution of measurements in both modes is ~50 km. The data are available for two seasons, winter and equinoxes, with no measurements for summer time. We consider here 5-min RISR data because they have much smaller errors in measurements than 1-min data that are available as well.

Figure 2 shows the total number of 5-min intervals of joint RISR-CLY radar measurements

125   for various UT. The number of the intervals was much larger during noon-dusk time (local solar noon is at about 19:00 UT). This is because of preferential occurrence of CLY echoes at ranges of interest during daytime (Ghezelbash et al., 2014). Unfortunately, not all available periods are suitable for the comparison. This is because the CLY data are often contaminated by ground scatter that profoundly affects the comparison, as shown recently by Gillies et al. (2018). Such periods

130   have been dropped from further consideration.

Our approach to the CLY-RISR velocity comparison is as follows. We first select 5-min period of RISR velocity measurements at latitudes of $\sim 71.625° - 73.125°$, see blue circles in Fig. 1, and compute median velocity value for RISR. We then consider median values of the CLY velocity over matched 5-min intervals in 3 beams and 4 gates, mentioned above. The matched data

135   are then entered into a common dataset.
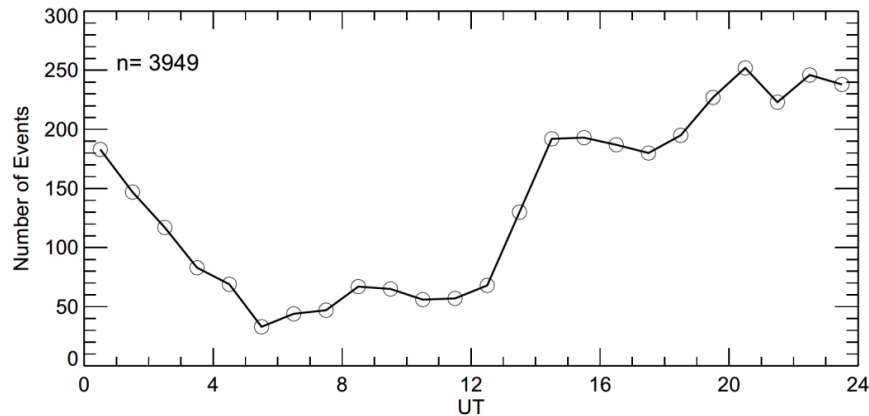
Figure 2: Number of CLY/RISR 5-min intervals of joint observations for all events considered. Total number of available intervals is shown in the top-left corner.

140

4 Results for CLY LOS velocity - RISR comparison

Figure 3a shows the CLY LOS velocity versus the RISR Eastward $\mathbf{E} \times \mathbf{B}$ component for the entire
145   dataset, produced as described above. The total number of points is close to 4000, which is a
significant number. Overall, both positive and negative velocities are well represented. Although
some spread in data is present, a significant amount of points is located close to the bisector of
perfect agreement. To assess the plot, we binned the data according to RISR measurements by
using 100-m/s bins. Binned in this way data are shown by black-white dots. The vertical black bars
150   crossing each dot are the binned CLY velocity value ± one standard deviation. We also binned the
data of Fig. 3 according to bins of the CLY velocity, pink asterisks (shown by thin symbols in
order not to contaminate the plot).
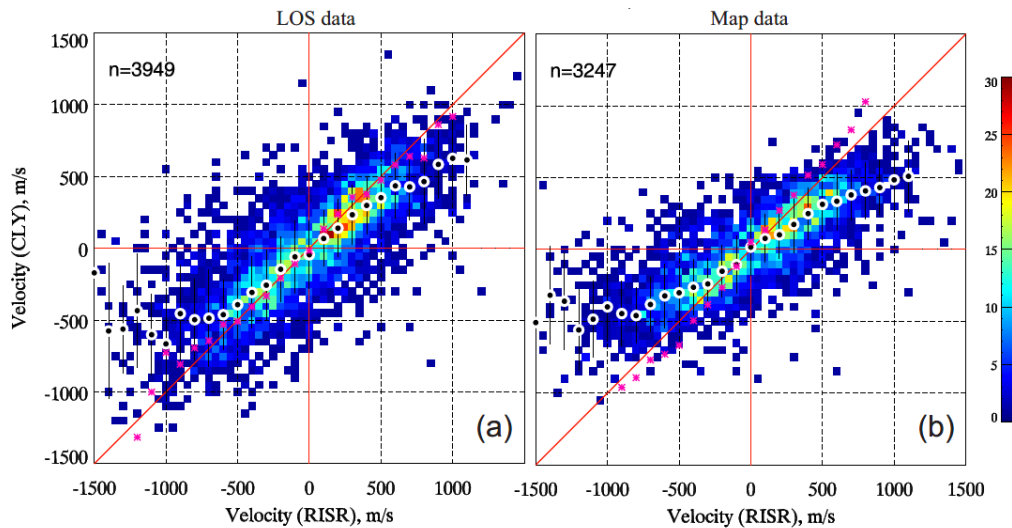
Figure 3: (a) Scatterplot of the CLY LOS velocity versus **E×B** eastward velocity component as inferred by RISR. Total number of points *n* is shown in the top left corner. The black-white dots are medians of the CLY velocity in 100-m/s bins of RISR velocity. The black vertical lines are the standard deviations of the CLY velocity in each bin. The pink dots are medians of the RISR velocity in 100-m/s bins of CLY measurements (b) The same as (a) but the flow eastward component inferred from SuperDARN flow maps was considered.

The black-white dots are reasonably close to the line of the perfect agreement. The pink asterisks are actually very close to the bisector line. Good alignment with the bisector and not very strong differences between the location of the black dots and pink asterisks indicate that the velocities are related almost linearly, especially in the range from -500 m/s to +500 m/s. One clear departure of the back dots from the bisector is at large RISR velocity magnitudes of > 750 m/s. If one to describe the dependence by a linear fit line between velocities of ± 1000 m/s, the slope of the fit line is ~0.65.

5 Methodology of "vector" comparison between SuperDARN and RISR

The approach to the velocity vector comparison between the RISR and SuperDARN data is as follows. We restrict the consideration to the same area of joint CLY-RISR observations as in the LOS comparison, Fig. 1. Here the SuperDARN convection vectors are available at geomagnetic latitudes of 80.5° − 81.5° and ~ 7° of magnetic longitude. We selected 3 closest (to the area of CLY LOS velocity assessment) grid nodes locations at MLAT=81.5° and 2 closest grid nodes

located at MLAT$=80.5°$, as indicated in Fig. 1 by red crosses. For each vector location, an astward component of the flow was computed and the median value (out of potentially 5 values, although for some periods it was as low as 1 measurement) was selected as a representative value of the eastward plasma flow component according to a specific SuperDARN map. In terms of time,

180 because RISR measurements considered had ~5-min resolution, standard SuperDARN convection maps with 5-min integration time were produced. This is not a traditional temporal resolution for the SuperDARN mapping (which is 2 min); such data processing has been done to avoid the need of additional averaging of 2-min SuperDARN maps. Unfortunately, the beginnings of RISR measurement intervals were often at irregular time while SuperDARN maps were produced over

185 exact time slots such as 0-5 min, 10-15 min and so on. For comparison, only data from the two systems that were less than 2 min apart were considered. For this reason, even when both radar systems were operational, the actual number of joint points per hour was below the expected number of 12.

For RISR, the eastward $\mathbf{E} \times \mathbf{B}$ velocity component has been usually available in all points

190 shown by open circles in Fig. 1. For the comparison with SuperDARN vectors, only measurements at geographic latitudes between $71.625° - 73.125°$ (given with a step of $0.25°$, blue-colored circles in Fig. 1) were considered, and the median value of the eastward component was computed. Obtained data pairs were entered into a common dataset for all the events available. We ended up with a slightly shorter data set than that for the LOS velocity comparison. We stress that although

195 the data for the comparison were along one specific direction, geographic east, two-dimensional vectors were used in determination of the velocity component for both systems.

6 Results for "vector" comparison between SuperDARN and RISR

200 Figure 3b plots eastward component of the plasma flow according to the two systems. The data spread looks similar to that of Fig. 3a (the LOS comparison). We assessed the plot of Fig. 3b by binning the data similarly to Fig. 3a, see open circles. Overall agreement of the data clearly holds.

Several details of the data of Fig. 3b are consistent with the data of Fig. 3a. First, the SuperDARN map-based velocities are somewhat smaller than those of RISR. This is recognizable

205 through an obvious deviation of the distribution maxima from the bisector of ideal agreement, especially at RISR positive velocities of > 500 m/s. If one to describe the dependence by a linear

fit line to the velocity medians in bins (open circles) between ± 1000 m/s, the slope of the fit line is 0.54. Secondly, the tendency of having smaller SuperDARN velocity is progressively stronger at larger RISR magnitudes. This feature is seen for both positive and negative RISR velocities.

210 Finally, consistent with previous reports (Koustov et al., 2016; Gillies et al., 2018), there is a number of points for which the radars show opposite velocity polarity; This was more frequent for small RISR velocities. Although the plot of Fig. 3 shows good consistency of the data provided by the two radar systems; the differences can be as large as a factor of 2 in individual measurements.

The agreement between the convection vectors given by RISR and SuperDARN is highly
215 expected. We see that the consistency deteriorates once 2-D data are involved, but mostly at intermediate velocity magnitudes of 300-600 m/s with the SuperDARN velocities being slower. Interestingly, the differences for large velocity magnitudes in Fig. 3b are comparable to those in Fig. 3a. We think that the deterioration of the agreement at intermediate velocity magnitudes is due to the broader area of SuperDARN data averaging for the 2-D comparison. In this case, there
220 are more chances for SuperDARN to involve ground-scatter contaminated measurements giving effectively slower grid velocities to the fitting procedure.

7. On possible reasons for velocity disagreements

225 One popular opinion about SuperDARN velocity measurements is the systematic "underestimation" of the velocity by the radars due to the assumption for the index of refraction to be one in HF measurements (starting from Gillies et al., 2009 and Ponomarenko et al., 2009). We attempted to evaluate the importance of this effect on our data set. A plot similar to that of Fig. 3a was produced, but with the CLY velocity being corrected by considering the electron density
230 (at the F region peak) measured by RISR. The plot looked very much similar to that of Fig. 3a. We assessed the plot by applying the linear fit line to the HF velocity medians in 100-m/s bins of RISR velocity, considering the range of almost linear dependence, between -1000 and +1000 m/s of RISR velocities. The slope of the best fit line improved to ~0.75 (from ~0.65). This improvement is consistent with the previous studies except the slope is not quite close to 1. We also investigated
235 the diurnal variation of the velocity ratio $R = {Vel_{HF}}/{Vel_{RISR}}$. Gillies et al. (2018) plotted R against

UT time considering the RKN SuperDARN radar. The idea is that the HF velocity decrease due to

the index of refraction effect should be strongest whenever the electron density in the scattering volume is highest. For the winter/equinoctial ionosphere over Resolute Bay, the largest densities are systematically observed at near local solar noon and afternoon hours (18-22 UT) (e.g.

240 Ghezelbash et al., 2014; Themens et al., 2017). It is therefore expected that the velocity ratio R would be smallest at near noon/afternoon hours, and this is what has been reported by Gillies et al. (2018) for the RKN radar. The nighttime results by Gillies et al. (2018) are more confusing. First, strangely, the ratios here were often above 1 at latitudes southward of RB and systematically below 1 (but not as strong as at near noon hours) at latitudes poleward of RB. Gillies et al. (2018)

245 indicated that the vertical plasma flow velocities in RISR measurements were, very likely, estimated not correctly for nighttime observations. Since the observation area in our comparison is close to RB, we can expect that this effect can also affect the RISR-CLY comparison.

Figure 4 plots the hourly-median ratio R as a function of time for our CLY-RISR data set. One can see that R varies significantly. It is decreased during daytime (noon is at about 19:00 UT)

250 as compared to that of dawn/prenoon hours (12-18 UT), but the values are smallest during nighttime (midnight is at about 07 UT). Interestingly, the average ratio over all UTs is 0.83, which is closer to 1 than the slopes of the lines in Figs. 3. This is probably because infrequent high-velocity data are averaged out by dominating data at low velocities in certain bins of Fig. 4.

We think that the low nighttime R values are resulted from "overestimation" of true plasma

255 drift in a plane perpendicular to the magnetic field by RISR in the midnight sector. We note that this is not quite consistent with Gillies et al. (2018) who interpreted their nighttime data in terms of effectively decreased RISR LOS velocities while our data suggest effectively increased RISR velocity magnitudes.

Gillies et al. (2018) believe that large nighttime ratios of RKN to RISR velocity could be

260 due to errors in HF measurements because the RKN beams can experience significant lateral deviations. This explanation cannot be applied to our observations. This is because the CLY radar observes azimuthally, along the average plasma flow most of the time (except of short periods at near noon and near midnight when the flows are predominantly meridional) so that lateral deviations of the CLY beams would give both smaller and larger velocity magnitudes.

265
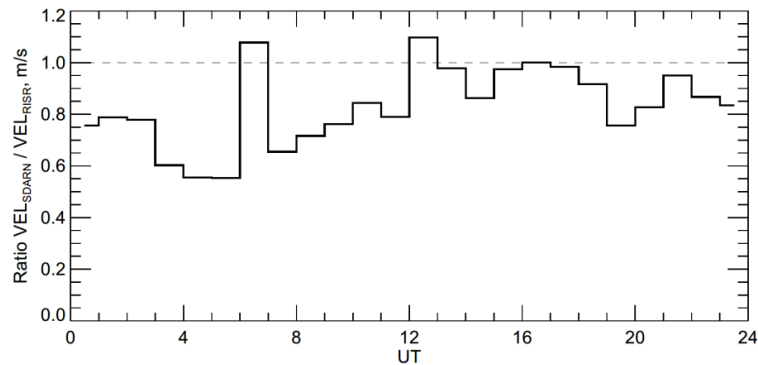
Figure 4: Line plot of the hourly median velocity ratio R versus UT for the CLY radar. The data set is the same as for Fig. 3a.

270   We think that the HF-RISR velocity inconsistency can also originate, at least partially, from the nature of HF signal formation. The effect has been discussed in general terms by Uspensky et al. (1989) as applied to E region coherent scatter and by Koustov et al. (2016) for F region coherent backscatter. The flows in the nighttime ionosphere are very likely to be more patchy/grainy with occasional occurrence of regions with enhanced flow magnitude (low electron

275   density) and decreased flow magnitude (high electron density). We argue that in a case of the patchy ionosphere, there is a good chance that the ratio R would be smaller as compared to the case of uniform ionosphere and homogeneous flow. Flow enhancements/decreases affect both RISR and HF measurements but in a profoundly different manner. RISR radar would average the velocity in patches with enhanced and depleted electron density equally, and it would report what

280   can be classified as the "background" flow velocity. In the presence of electron density patches with enhanced and decreased $\mathbf{E} \times \mathbf{B}$ flows, HF radars would preferentially detect stronger signals from those areas where the electron density is enhanced, and the electric field (flow magnitude) is decreased so that it would show somewhat smaller velocity than the background value measured by an incoherent scatter radar.

285   It is conceivable to have an opposite situation with HF velocities above the background flow if regions with enhanced density have stronger local electric field, as discussed in Uspensky et al. (1989). In this respect, Koustov et al. (2016) and Gillies et al. (2018) noticed that HF velocities could be larger than the $\mathbf{E} \times \mathbf{B}$ drift component measured by ISRs. Occasional such points are seen in previously published data, for example in Ruohoniemi et al. (1987) and Davies

290   et al. (1999). Our data of Fig. 3 also show such points but, overall, the data agree. Although both

Koustov et al. (2016) and Gillies et al. (2018) related the effect to lateral deviations of the HF radar beams from the expected directions, it partially could be due to the above effect of ionospheric microstructuring.

Potentially, low *R* values can be related to the occurrence of misidentified ionospheric
295 scatter because some ionospheric echoes with low velocities can actually be ground or mixed scatter. Gillies et al. (2018) showed that removal of points that could potentially be affected by ground scatter improves the RKN-RISR velocity agreement significantly. Our analysis showed that ground scatter is rare during winter/equinox nighttime for the CLY radar which is consistent with low nighttime F region densities (Ghezelbash et al., 2014; Themens et al., 2017). We also
300 have to remind that obvious periods with CLY ground scatter contamination have been removed from our consideration in Fig. 3.

Investigating our database, we identified one special situation when the RISR-SuperDARN velocity disagreements were particularly strong. Figure 5 gives an example of CLY-RISR observations on 4 March 2016 where RISR and CLY velocities differ consistently by several
305 hundred m/s over a period of almost 2 hours.
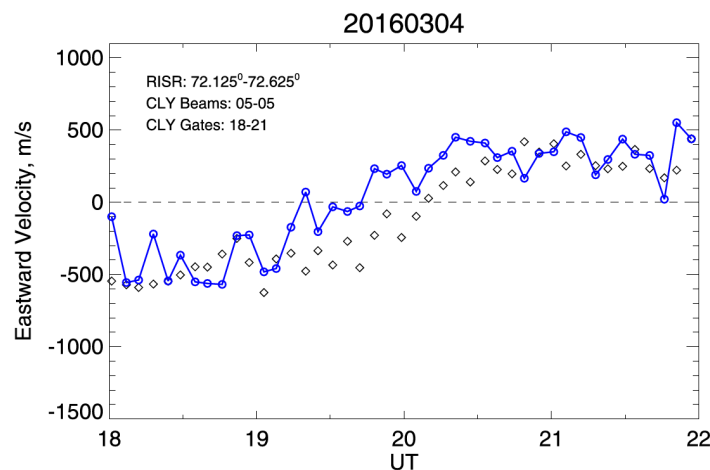
Figure 5: Eastward component of the **E×B** drift as measured by RISR (red diamonds, 5-min
310 resolution data) and matched velocity medians of CLY observations (5-min medians of original 1-min measurements in beams/gates "overlapping" the region of RISR observations) for the event of 04 March 2016.

Figure 6a illustrates, just for one CLY velocity scan, the typical spatial velocity distribution

315   within the radar FoV, for the above event. A sharp change in the LOS velocity polarity from
positive values in low number beams to negative values in high number beams is noticeable. The
polarity transition occurs in the central beams 5-7. Figure 6b gives a global-scale map of plasma
flow inferred from all SuperDARN radar measurements. The map has a number of vectors
originated from the RKN and INV radar measurements on a top of those from CLY measurements.

320   Presence of highly-curved flows is evident at near noon hours. Under these conditions, both
SuperDARN and RISR can have difficulties in the construction of a 2-D vector field.
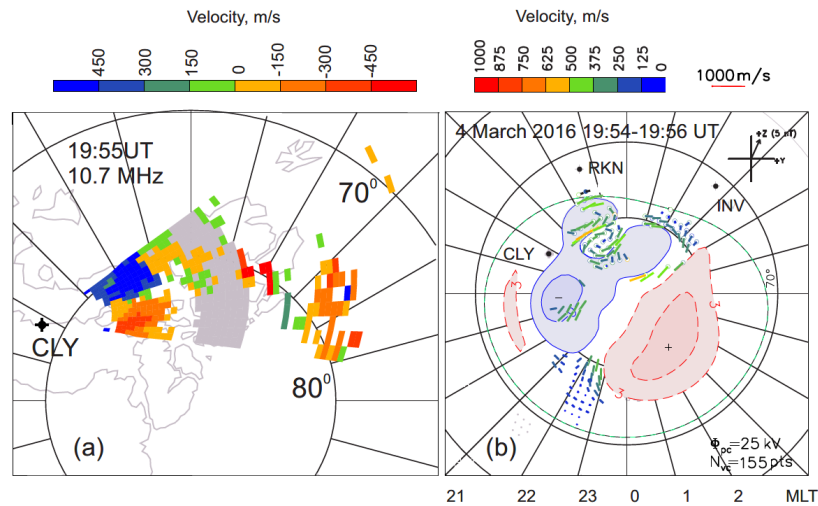
Figure 6: (a) A CLY LOS velocity map at 19:55 UT on 04 March 2016 and (b) a standard 2-min
convection maps inferred from all SuperDARN radar measurements for the same period of time.

325

We comment that the flows seen in Fig. 6 are sunward, roughly along the magnetic
meridian at near noon hours, signifying the occurrence of a reverse convection cell. This is highly
expected since the IMF B_z was steady at about +5 nT starting from 18:30 UT all the way until ~22
UT for this event.

330   Evaluation of the extent the SuperDARN and RISR vectors are affected by the shear in the
flow is difficult. We realized visually that the centers (foci) of the convection cells, according to
RISR and SuperDARN, do not coincide in latitude for many cases in this event.   In addition, we
realized that, while selecting the SuperDARN map data at lower latitudes, the agreement between
the RISR and SuperDARN map data improves dramatically.

335   To investigate further, we determined the location of the convection reversal boundary
(CRB) for the reverse convection cell (like that shown in Fig. 6b) by considering the standard 2-
min SuperDARN maps, CLY velocity-scan maps and by looking at the reversal in the latitudinal
profile of the RISR velocity (these are given for 5-min intervals). The data are presented in Fig. 7.
One feature is obvious here: the CRB is located at almost 2° larger MLAT for SuperDARN at the

340   beginning of the event, and the differences are minimal toward the end of the event. Plotted in Fig.
7 the CRB location according to solely CLY velocity-scan maps is closer to that inferred from
RISR data hinting that perhaps the SuperDARN fitting procedure is the major factor for strong
differences between the SuperDARN maps and RISR measurements in this specific event. This is
not to say that RISR measurements are exact; they are very likely also subject to errors under these

345   strongly-curved flows.
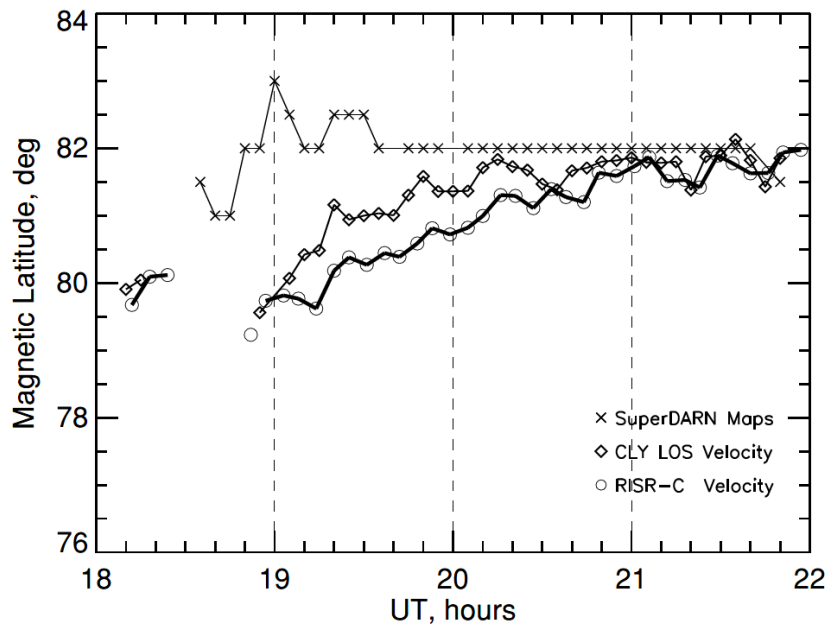
Figure 7: Magnetic latitude of the flow reversal location within the dayside reverse convection
cell as inferred from SuperDARN convection maps (crosses), CLY LOS velocity measurements
350   in various beams (diamonds) and RISR measurements for the event of 04 March 2016.

Summary and conclusions

In this study, we attempted to validate the CLY SuperDARN radar velocity measurements by comparing them with the data collected by the Resolute Bay incoherent scatter radar. Because no line-of-sight velocity comparison is possible for the geometry of joint observations, we adopted here a different approach, namely we considered eastward component of $\mathbf{E}\times\mathbf{B}$ flow vector as inferred from RISR measurements in multiple beams and compared it with either CLY velocities in a number of beams oriented eastward or with the eastward component of the plasma flow inferred from 2-D SuperDARN maps. The analysis undertaken allows us to make several conclusions.

1. The CLY radar velocity measured in beams 4-6 is statistically comparable to the $\mathbf{E}\times\mathbf{B}$ component of the plasma drift along these beams (eastward/azimuthal plasma flows) as measured by the RISR incoherent scatter radar. This implies that the velocity data provided by the CLY radar to the SuperDARN database are reliable and suitable for convection mapping involving all SuperDARN radars. The comparisons performed are an addition to the previous validation work for the RKN and INV SuperDARN radars.

2. The slope of the best linear fit line to the CLY velocity variation versus $\mathbf{E}\times\mathbf{B}$ component (as measured by RISR) applied to the binned values is on the order of 0.65 if all the available data (removing data with obvious ground-scatter contamination) in the range ± 1000 m/s are considered. Correction of HF velocities on the index of refraction effect improves the slope to ~0.75. The slope of the linear fit line for the corrected data is still below 1 implying that additional factors affect the relationship. Additionally, diurnal variation of the ratio of HF velocity to the RISR velocity shows strongest decrease below 1 during nighttime and not daytime.

3. The effect of HF velocity underestimation for the CLY radar becomes progressively stronger for faster plasma drifts above ~750 m/s.

4. It is suggested that one of these additional factors is a bias in HF radar measurements of the velocity because HF radars get stronger signals from ionospheric regions with enhanced electron

density where the electric field/$\mathbf{E} \times \mathbf{B}$ drift can be decreased as compared to the background plasma.

5. In a case of highly-sheared plasma flows, such as near dayside reverse convection cells

390   occurring under strong IMF $B_z > 0$, the differences between RISR and SuperDARN velocity vectors can be large.

6. Reasonable agreement between the velocities of the two systems implies that the RISR technique of the $\mathbf{E} \times \mathbf{B}$ derivation from multiple individual radar beams is a reliable method most

395   of the time. The comparison suggests that the RISR vectors are less reliable in the midnight sector where the flows are often very irregular, and strong vertical motions occur.

400   **Acknowledgments**

Continuous funding of SuperDARN radars by National Scientific Agencies of Australia, Canada, China, France, Italy, Japan, Norway, South Africa, United Kingdom, and the United States of America is appreciated. The current research would be impossible without ongoing support from the Canadian Foundation for Innovation, Canadian Space Agency's Geospace Observatory (GO

405   Canada) continuation initiative to the U of Saskatchewan radar group and NSERC Discovery grant to A.V.K. The University of Calgary RISR-C radar is funded by the Canada Foundation for Innovation and is a partnership with the US National Science Foundation and SRI International. We thank C. Graf for the initial analysis of RISR density data and R. Fiori for the help in software development. Discussions of various aspects of the paper with P. V. Ponomarenko and his help in

410   software development are appreciated.

415

References

420

Bahcivan, H., Nicolls, M. J., and Perry, G.: Comparison of SuperDARN irregularity drift measurements and F-region ion velocities from Resolute Bay ISR, J. Atmos. Solar Terr. Phys., 105-106, 325–331, https://doi.org/10.1016/j.jastp.2013.02.002, 2013.

425 Davies, J., Lester, M., Milan, S. E., and Yeoman, T.: A comparison of velocity measurements from the CUTLASS Finland radar and the EISCAT UHF system, Ann. Geophys., 17, 892-902, https://doi.org/10.1007/s00585-999-0892-9, 1999.

Ghezelbash, M., Koustov, A. V., Themens, D. R., and Jayachandran, P. T.: Seasonal and diurnal
430 variations of PolarDARN F region echo occurrence in the polar cap and their causes, J. Geophys. Res. Space Physics, 119, https://doi:10.1002/2014JA020726, 2014.

Gillies, R. G., Hussey, G. C., Sofko, J. G., McWilliams, K. A., Fiori, R. A. D., Ponomarenko, P. V., and St.-Maurice, J.-P.: Improvement of SuperDARN velocity measurements by estimating the index of refraction in the scattering region using interferometry, J. Geophys. Res., 114, A07305,
435 https://doi:10.1029/2008JA013967, 2009.

Gillies, R. G., Hussey, G. C., Sofko, G. J., Wright, D. M., and Davies, J. A.: A comparison of EISCAT and SuperDARN F-region measurements with consideration of the refractive index in the scattering volume, J. Geophys. Res., 115, A06319, https://doi:10.1029/2009JA014694, 2010.

440

Gillies, R. G., van Eyken, A., Spanswick, E., Nicolls, M. J., Kelly, J., Greffen, M., Knudsen, D., Connors, M., Schutser, M., Valentic, T., Malone, M., Buonocore, J., St.-Maurice, J.-P., and Donovan, E.: First observations from the RISR-C incoherent scatter radar, Radio Sci., 51, 1645-1659. https://doi:10.1002/2016RS006062, 2016.

445

Greenwald, R. A., Baker, K. B., Dudeney, J. R., Pinnock, M., Jones, T. B., Thomas, E. C., Villain, J.-P., Cerisier, J.-C., Senior, C., Hanuise, C., Hunsuker, R. D., Sofko, J. G., Koehler, J. A., Nielsen, E., Pellinen, R., Walker, A. D. M., Sato, N., and Yamagishi, H.: DARN/SuperDARN: A global view of the dynamics of high-latitude convection, Space Sci. Rev., 71, 761-796, https://doi:
450 10.1007/BF00751350, 1995.

Heinselman, C. J., and Nicolls, M. J.: A Bayesian approach to electric field and E-region neutral wind estimation with the Poker Flat Advanced Modular Incoherent Scatter Radar, Radio Sci., 43, RS5013, https://doi:10.1029/ 2007RS003805, 2008.

455

Koustov, A. V., St-Maurice, J.-P., Sofko, G. J., Andre, D., McDougall, J. W., Hairston, M. R., Fiori, R. A., and Kadochnikov, G. E.: Three-way validation of the Rankin Inlet PolarDARN radar velocity measurements, Radio Sci., 44, RS4003, https://doi:10.1029/2008RS004045, 2009.

460 Koustov, A. V., Lavoie, D. B., and Varney, R. H.: On the consistency of the SuperDARN radar velocity and $E \times B$ plasma drift, Radio Sci., 51, 1792–1805, https://doi:10.1002/2016RS006134, 2016.

Milan, S. E., Davies, J. A., and Lester, M.: Coherent HF radar backscatter characteristics associated with auroral forms identified by incoherent radar techniques: A comparison of CUTLASS and EISCAT observations, J. Geophys. Res., 104, 22591–22604, https://doi:10.1029/1999JA900277, 1999.

465

Mori, D., Koustov, A. V., Jayachandran, P. T., and Nishitani, N.: Resolute Bay CADI ionosonde drifts, PolarDARN HF velocities and SuperDARN cross polar cap potential, Radio Science, 47, RS3003, https://doi:10.1029/2011RS004947, 2012.

470

Ruohoniemi, J. M., and Baker, K. B.: Large-scale imaging of high-latitude convection with Super Dual Auroral Radar Network HF radar observations, J. Geophys. Res., 103, 20797-20811, https://doi: 10.1029/98JA01288, 1998.

Ponomarenko, P. V., St.-Maurice, J.-P., Waters, C. L., Gillies, R. G., and Koustov, A.V.: Refractive index effects on the scatter volume location and Doppler velocity estimates of ionospheric HF backscatter echoes, Ann. Geophys., 27, 1-13, https://doi.org/10.5194/angeo-27-4207-2009, 2009.

475

Ruohoniemi, J. M., Greenwald, R. A., Baker, K. B., Villain, J.-P., and McCready, M. A.: Drift motions of small-scale irregularities in the high-latitude F region: An experimental comparison with plasma drift motions, J. Geophys. Res., 92, 4553-4564, https://doi.org/10.1029/JA092iA05p04553, 1987.

480

Shepherd, S. G., and Ruohoniemi, J. M.: Electrostatic potential patterns in the high-latitude ionosphere constrained by SuperDARN measurements, J. Geophys. Res., 105, 23,005-23,014, https://doi.org/10.1029/2000JA000171, 2000.

485

Themens, D. R., Jayachandran, P. T., Galkin, I., and Hall, C.: The Empirical Canadian High Arctic Ionospheric Model (E-CHAIM): NmF2 and hmF2, J. Geophys. Res. Space Physics, 122, 9015–9031, https://doi:10.1002/2017JA024398, 2017.

490

Uspensky, M. V., Koustov, A. V., Williams, P. J. S., Huuskonen, A., Kangas, J., and Nielsen, E.: Effect of unresolved electrojet microstructure on measurements of irregularity drift velocity in auroral radar backscatter, Adv. Space Res., 9, 119-122, https://doi.org/10.1016/0273-1177(89)90349-9, 1989.

495

Xu, L., Koustov, A., Thayer, J., and McCready, M.: SuperDARN convection and Sondrestrom plasma drift, Ann. Geophys., 19, 749-759, https://doi.org/10.5194/angeo-19-749-2001, 2001.

500

Author contributions.
RG and PB worked on raw data processing and their preliminary analysis. PB prepared some diagrams. AVK did most of the comparison work and wrote the initial manuscript. All authors participated in the writing, and all commented on the paper.

505